Diagnosis of boundary-layer circulations

Robert J. Beare and Michael J. P. Cullen

Diagnoses of circulations in the vertical plane provide valuable insights into aspects of the dynamics of the climate system. Dynamical theories based on geostrophic balance have proved useful in deriving diagnostic equations for these circulations. For example, semi-geostrophic theory gives rise to the Sawyer-Eliassen equation (SEE) that predicts, amongst other things, circulations around mid-latitude fronts. A limitation of the SEE is the absence of a realistic boundary layer. However, the coupling provided by the boundary layer between the atmosphere and the surface is fundamental to the climate system. Here we use a theory based on Ekman momentum balance to derive a Sawyer-Eliassen equation which includes a boundary layer (SEEBL).

We consider a case-study of a baroclinic low-level jet. The SEEBL solution shows significant benefits over Ekman pumping including accommodating a boundary-layer depth which varies in space and structure which accounts for buoyancy and momentum advection. The diagnosed low-level jet is stronger than that determined by Ekman balance. This is due to the inclusion of momentum advection. Momentum advection provides an additional mechanism for enhancement of the low-level jet which is distinct from inertial oscillations.

Key words: Boundary layer. Circulation. Ekman balance. Advection. Sawyer-Eliassen equation. Low-level jet.

:

1. Introduction

The climate system consists of phenomena on a large range of spatial and temporal scales. In climate models, spatial scales that are resolved by the grid scale can typically be represented by its advective dynamics. In addition there is a large range of important processes with scales smaller than the grid scale; examples of these processes are: radiation, moist convection, land-surface heterogeneity and boundary-layer turbulence. These processes are represented by sub-grid parametrizations. A challenge for climate modelers is understanding the coupling between the sub-grid parametrizations and the resolved dynamics. It is arguable that such coupling has received much less research effort relative to the separate development of the dynamical core and parametrizations. Here, we focus around the important case of the coupling between the atmosphere and the ocean or land surface. This is very important, and is achieved primarily through heat, moisture and momentum transfers within the atmospheric boundary layer.

Our approach to understanding the coupling between the dynamics and the boundary layer is to consider regimes where the two are close to a state of balance. Our understanding of the large-scale atmosphere and ocean circulations has been greatly helped by the realisation that they are close to a state of

Proc. R. Soc. A 1–18; doi: 10.1098/rspa.00000000

geostrophic balance (pressure gradients balancing Coriolis force). The quasi- semi- and planetary geostrophic models extend the steady state balance assumptions to include non-stationarity and advection. Following the seminal works of Sawyer (1956) and Eliassen (1962), the Sawyer-Eliassen equation (SEE) diagnoses the ageostrophic circulations forced by advection of heat and momentum. The SEE has proved invaluable in describing the dynamics of meteorological fronts. Subsequently, Hoskins (1975) defined the semi-geostrophic theory from which the SEE can be derived.

A weakness of the SEE is that it lacks a representation of the atmospheric boundary layer. Inclusion of the effects of turbulent diffusion would thus be valuable in understanding the coupling between the boundary-layer parametrization and the dynamics in both climate and weather prediction models. The aim of this paper is to form a diagnostic equation named the SEEBL, Sawyer-Eliassen equation including a boundary layer, for circulations in the vertical plane. Analogous to the SEE, we will assume that the boundary layer is close to a state of balance, but now we use the Ekman balance (pressure gradient, Coriolis and boundary layer drag in balance). Such a balance has been used in diagnosing Ekman pumping for cyclone systems (Beare, 2007) or ocean gyres and convergence in the tropics (Back and Bretherton, 2009). However, the extension to include non-stationarity and advection has been less utilised. Beare and Cullen (2010) and Beare and Cullen (2012) demonstrated the use of time-varying models based on Ekman balance for stratified and shallow water systems respectively. They also demonstrated the utility of the semi-geotriptic (SGT) model, directly analogous to the semi-geostrophic model but with a realistic boundary layer included.

Low-level jets are a significant feature of atmospheric behaviour. They contribute to extremes such as very high winds in extra-tropical cyclones (Clark *et al.*, 2005), and heavy rainfall (Chen *et al.*, 2005). Low-level jets also feature a combination of dynamical, moisture and boundary-layer forcings. It is typically observed that low-level jets have a significant ageostrophic component (e.g. Akiyama, 1973). Here we will aim to expand on this observation by using a theory that defines the dynamics relative to the Ekman-balanced wind rather than the geostrophic wind.

First we will derive the SGT equations from the primitive equations, also describing the regime for which they are valid (section 2). In section 3, the SEEBL will then be derived from the SGT equations. We will then give example numerical solutions of the SEEBL for a mid-latitude low-level jet, and show the benefits of this new equation in describing the coupling to the interior dynamics.

2. The semi-geotriptic equations

In this section we derive the semi-geotriptic (SGT) equations which are the basis of the SEEBL diagnostic circulation equation.

(*a*) *Primitive equations including boundary layer parametrization*

We start our analysis with the two dimensional, Boussinesq, hydrostatic primitive equations (HPEs) on an f-plane, including boundary-layer terms:

$$\frac{Du}{Dt} - fv + \frac{\partial \phi}{\partial x} = \frac{\partial}{\partial z}\left(K_m \frac{\partial u}{\partial z}\right) \tag{2.1}$$

$$\frac{Dv}{Dt} + fu = \frac{\partial}{\partial z}\left(K_m \frac{\partial v}{\partial z}\right) \tag{2.2}$$

$$\frac{\partial \phi}{\partial z} = b \tag{2.3}$$

$$\frac{Db}{Dt} = \frac{\partial}{\partial z}\left(K_h \frac{\partial b}{\partial z}\right) = F_b \tag{2.4}$$

$$\frac{\partial u}{\partial x} + \frac{\partial w}{\partial z} = 0 \tag{2.5}$$

$$\frac{D}{Dt} = \frac{\partial}{\partial t} + u\frac{\partial}{\partial x} + w\frac{\partial}{\partial z} \tag{2.6}$$

The symbols used above are defined in Table 1. The terms on the right-hand side of Eqs. (2.1), (2.2) and (2.4) represent the forcing due to the boundary layer. The boundary layer is represented by vertical diffusion terms on the basis that the boundary layer depth is much less than the horizontal scale of interest. Here we confine our analysis to stratified and near-neutral flows in the boundary layer. We use a first-order closure for stratified and near-neutral boundary layers used in many numerical weather prediction models (Louis, 1979). Here, the vertical diffusivities of momentum and heat are expressed as a function of a mixing length (λ), the vertical wind shear (S) and functions of gradient Richardson number (Ri):

$$K_m = \lambda^2 S f_m(Ri) \quad K_h = \lambda^2 S f_h(Ri) \tag{2.7}$$

where f_m and f_h are stability functions for momentum and heat respectively. The boundary-layer mixing is controlled by the 'long-tails' function, which has the form:

$$f_m(Ri) = Pr\, f_h(Ri) = \frac{1}{1 + 10Ri} \quad Ri \geq 0 \quad Pr = 0.7 \tag{2.8}$$

where Pr is the neutral Prandtl number. Whilst many theoretical studies assume that K_m is constant, here we use a realistic diffusivity which is a function of both space and time.

(*b*) *Ekman balance limit of HPEs*

Given a boundary-layer frictional timescale, τ_f, and the advective timescale, T, we can define a small dimensionless parameter, ϵ:

$$\epsilon = \frac{\min[f^{-1}, \tau_f]}{T} \tag{2.9}$$

The min operation is designed to capture the fastest process out of the Coriolis and the boundary-layer friction. In the limit of zero ϵ, advection is negligible with

Symbol	Meaning
(x, z, t)	Cartesian coordinates and time
(u, v, w)	Wind vector
f	Coriolis parameter (constant)
ϕ	Geopotential
b	Buoyancy
K_m	Boundary-layer vertical momentum diffusivity
K_h	Boundary-layer vertical thermal diffusivity
F_b	Boundary-layer buoyancy tendency

Table 1. Symbols used in Eqs (2.1) - (2.6). All variables are a function of (x, z, t).

respect to the Coriolis, pressure-gradient and boundary-layer friction forces in Eqs (2.1) and (2.2), giving the zero-order Ekman balance:

$$-fv_e + \frac{\partial \phi}{\partial x} = \frac{\partial}{\partial z}\left(K_m \frac{\partial u_e}{\partial z}\right) \tag{2.10}$$

$$fu_e = \frac{\partial}{\partial z}\left(K_m \frac{\partial v_e}{\partial z}\right) \tag{2.11}$$

The components of the Ekman-balanced wind are u_e and v_e (hence the subscript 'e'). The Ekman-balanced wind is also sometimes called the 'geotriptic' (Earth rubbing) wind. When the boundary-layer momentum diffusivity is zero, Eqs (2.10) and (2.11) revert to geostrophic balance, so also apply above the boundary layer.

The frictional thermal wind balance in the x direction is formed by taking $\frac{\partial}{\partial z}$ of Eq. (2.10) and substituting from for $\frac{\partial \phi}{\partial z}$ from Eq. (2.3):

$$f\frac{\partial v_e}{\partial z} - \frac{\partial b}{\partial x} = -\mathcal{D}\frac{\partial u_e}{\partial z} \tag{2.12}$$

where the vertical diffusion operator, $\mathcal{D}$, applied to an an arbitrary function, g, is written as $\mathcal{D}g = \frac{\partial^2}{\partial z^2}(K_m g)$.

(*c*) *Derivation of SGT equations*

We now consider the case where ϵ is *non-zero* and advection is no longer negligible. We expand the horizontal winds in Eqs (2.1) and (2.2) as an asymptotic expansion in ϵ about Ekman balance.

$$\begin{gathered} u = u_e + u_1 + O(\epsilon^2 u_e) \\ v = v_e + v_1 + O(\epsilon^2 v_e) \\ |u_1| = \epsilon |u_e| \quad |v_1| = \epsilon |v_e| \end{gathered} \tag{2.13}$$

The terms in Eq. (2.13) are expressed as successive powers of ϵ. Substituting Eq. (2.13) into Eqs (2.1) and (2.2) and retaining terms of order $\epsilon|u_e|$ and $\epsilon|v_e|$

respectively gives:

$$\frac{Du_e}{Dt} - f(v - v_e) = \frac{\partial}{\partial z}\left(K_m \frac{\partial(u - u_e)}{\partial z}\right) \tag{2.14}$$

$$\frac{Dv_e}{Dt} + f(u - u_e) = \frac{\partial}{\partial z}\left(K_m \frac{\partial(v - v_e)}{\partial z}\right) \tag{2.15}$$

Whilst this is typically the end-point of the analysis for asymptotic expansion about the geostrophic wind (e.g. Pedlosky, 1987), there is an additional important consideration of stability when Ekman balance is used. For the approximation to be useful, it is necessary that Eqs (2.14) and (2.15) can be solved for $O(T\epsilon^{-1})$, long time, so that accuracy can be maintained. Whilst the diffusive terms in Eqs (2.14) and (2.15) are second-order accurate in ϵ, they lead to an unstable evolution of the domain integrated energy (E_{int}) in the absence of heating ($F_b = 0$):

$$\frac{dE_{int}}{dt} = -\int_0^{H_d}\int_{-L_d}^{L_d} K_m \left[2\frac{\partial u}{\partial z}\frac{\partial u_e}{\partial z} + 2\frac{\partial v}{\partial z}\frac{\partial v_e}{\partial z} - \left(\frac{\partial u_e}{\partial z}\right)^2 - \left(\frac{\partial v_e}{\partial z}\right)^2\right] dxdz \tag{2.16}$$

$$E_{int} = \int_0^{H_d}\int_{-L_d}^{L_d} \left[\frac{1}{2}(u_e^2 + v_e^2) - zb\right] dxdz \tag{2.17}$$

where the domain width and height are $2L_d$ and H_d respectively. The right-hand side of Eq. (2.16) is dependent on both (u, v) as well as (u_e, v_e) meaning that the energy evolution will not be robustly negative definite. For example, when $\frac{\partial u}{\partial z}$ and $\frac{\partial u_e}{\partial z}$ have opposite signs, E_{int} could grow instead of decay. Beare and Cullen (2012) provide more analysis of this situation. In order to maintain a negative definite energy tendency, the sign of the diffusive term needs to be reversed, giving the SGT equations:

$$\frac{Du_e}{Dt} - f(v - v_e) = \frac{\partial}{\partial z}\left(K_m \frac{\partial(u_e - u)}{\partial z}\right) \tag{2.18}$$

$$\frac{Dv_e}{Dt} + f(u - u_e) = \frac{\partial}{\partial z}\left(K_m \frac{\partial(v_e - v)}{\partial z}\right) \tag{2.19}$$

We note that the advecting wind (u) has a significant divergent component, including the Ekman-balanced wind u_e, so none of the terms in the thermodynamic equations can be neglected. The buoyancy equation used is thus:

$$\frac{Db}{Dt} = F_b \tag{2.20}$$

The domain integrated energy in the absence of heating is now negative definite:

$$\frac{dE_{int}}{dt} = -\int_0^{H_d}\int_{-L_d}^{L_d} K_m \left[\left(\frac{\partial u_e}{\partial z}\right)^2 + \left(\frac{\partial v_e}{\partial z}\right)^2\right] dxdz \tag{2.21}$$

This means that the second-order accuracy of Eqs (2.14) and (2.15) cannot be maintained in time, but first order accuracy of Eqs (2.18) and (2.19) can be maintained, so that diagnostics calculated from them will be meaningful. The inclusion of advection and inertial terms on the left-hand side of Eqs (2.18) and (2.19) and buoyancy advection in Eq. (2.20) still gives an improvement in accuracy

	Geostrophic balance	**Ekman (geotriptic) balance**
Steady state balances	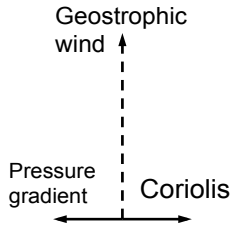	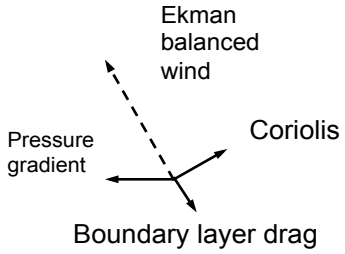
Prognostic models	Planetary geostrophic (PG) Semi-geostrophic (SG) Quasi-geostrophic (QG)	**Planetary-geotriptic (PGT)** **Semi-geotriptic (SGT)**

Figure 1. The balances above (left column) and within (right column) the boundary layer. Top row shows the steady state balances, and the bottom row the associated time-varying balanced models described in Section 2.

over simply using Ekman balance (Beare and Cullen, 2012). The SGT equations are also only accurate in the region of the boundary layer where Ekman balance is a good first approximation, above the surface layer (approximately the lowest 10% of the boundary layer).

(*d*) *Relationship to geostrophic models.*

Given L and U are typical scales for length and horizontal velocity respectively and assuming τ_f^{-1} is negligible above the boundary layer gives:

$$\epsilon = \frac{1}{fT} = \frac{U}{fL} = R_o \tag{2.22}$$

where R_o is the Rossby number. The appropriate zero-order balance is now geostrophic. Figure 1 compares both geostrophic and Ekman balances. When the advection of buoyancy and momentum is significant, we form the prognostic equations given in the second row of Fig. 1; the prognostic equations based on geostrophic balance are the familiar planetary, semi- and quasi- geostrophic equations. The SGT equations are the Ekman-balanced analogue of the semi-geostrophic (SG) equations. The reasons for this particular analogue in the boundary layer, as opposed to the quasi-geostrophic analogue, is that the SG thermodynamic equation includes all the advection terms.

3. Sawyer-Eliassen Equation including the Boundary Layer (SEEBL)

The Sawyer-Eliassen equation (SEE) is a linear diagnostic equation for the ageostrophic wind derived from the semi-geostrophic equations (Sawyer, 1956; Eliassen, 1962). In an analogous way, we will derive a Sawyer-Eliassen equation including a boundary layer using the semi-*geotriptic* (SGT) equations. We apply frictional thermal wind balance (Eq. 2.12) to Eqs (2.18)-(2.20) in order to eliminate the time derivatives of u_e, v_e and b. The resulting Sawyer-Eliassen equation including the boundary layer (SEEBL) is:

$$\left[f\left(f+\frac{\partial v_e}{\partial x}\right)+\mathcal{D}^2+\frac{\partial u_e}{\partial x}\mathcal{D}\right]\frac{\partial^2\psi}{\partial z^2}+N^2\frac{\partial^2\psi}{\partial x^2}$$
$$-\left(\frac{\partial u_e}{\partial z}\mathcal{D}-\mathcal{D}\frac{\partial u_e}{\partial z}+2\frac{\partial b}{\partial x}\right)\frac{\partial^2\psi}{\partial x\partial z}-\frac{\partial\mathcal{D}}{\partial x}\frac{\partial u_e}{\partial z}\frac{\partial\psi}{\partial z}$$
$$+\frac{\partial\mathcal{D}}{\partial z}\frac{\partial u_e}{\partial z}\frac{\partial\psi}{\partial x}=\left(f^2+\mathcal{D}^2+\frac{\partial\mathcal{D}}{\partial t}\right)\frac{\partial u_e}{\partial z}-\frac{\partial\mathcal{F}_b}{\partial x} \tag{3.1}$$

where N is the Brunt-Väisällä frequency $\left(N^2=\frac{\partial b}{\partial z}\right)$ and the stream function ψ is defined as:

$$(u,w)=\left(\frac{\partial\psi}{\partial z},-\frac{\partial\psi}{\partial x}\right) \tag{3.2}$$

The vertical velocity is zero on all the boundaries giving:

$$\frac{\partial\psi}{\partial x}=0 \quad \text{at } x=\pm L_d$$
$$\psi=0 \quad \text{at } z=0 \text{ and } z=H \tag{3.3}$$

Equation (3.3) is a free-slip surface boundary condition. A non-slip surface boundary condition ($\frac{\partial\psi}{\partial z}=0$) is ill-posed for an arbitrary forcing term on the right hand side of Eq. (3.1) and implies non-zero vertical velocity at the surface. As stated in section 2c, the diagnosed u from the SGT equations is accurate above the surface layer.

We will now consider the novel structure of Eq. (3.1). Whilst the SEE is in terms of the geostrophic wind, the SEEBL is in terms of the Ekman-balanced wind. The terms in $\frac{\partial v_e}{\partial x}$ and $\frac{\partial u_e}{\partial x}$ originate from the advection of momentum. The terms in N^2, $\frac{\partial b}{\partial x}$ and F_b represent a full coupling of the boundary layer to the buoyancy equation. In the limit of zero boundary-layer diffusion ($\mathcal{D}\to 0$), the left-hand side of the SEEBL then becomes that of the SEE. Sawyer-Eliassen equations are often solved with the Q-vector forcing on the right-hand side, for example due to frontal deformation (e.g. Thorpe and Nash, 1984). Whilst this is straightforward to include, we choose here to consider just the role of the boundary layer forcings in the circulation. Equation (3.1) is discretised using finite differences and solved using a standard sparse matrix solver. The solvability condition for the discretised SEEBL is:

$$\left[f\left(f+\frac{\partial v_e}{\partial x}\right)+D^2+\frac{\partial u_e}{\partial x}D\right]N^2-\frac{\partial b}{\partial x}^2>0 \tag{3.4}$$

where D represents the diagonal elements of the discretised $\mathcal{D}$ operator. The presence of the D^2 term makes the discretised SEEBL equation more positive definite than the SEE. Whilst the SEE is degenerate at the equator ($f=0$), the presence of the D terms means that the SEEBL can still diagnose a circulation at the equator.

By applying the balance in Eq.(2.11) to Eqs. (2.18) and (2.19) we can also diagnose v:

$$(f^2+d^2)v = \left(f^2+d^2+\frac{\partial d}{\partial t}\right)v_e - d\left(u\frac{\partial v_e}{\partial x}+w\frac{\partial v_e}{\partial z}\right)+f\left(u\frac{\partial u_e}{\partial x}+w\frac{\partial u_e}{\partial z}\right) \tag{3.5}$$

where $d(g)=\frac{\partial}{\partial z}\left(K_m\frac{\partial g}{\partial z}\right)$, $v=0$ at $z=0$ and $v=v_g$ at $z=H$ (v_g is the geostrophic wind in the y-direction).

(*a*) *Other approaches*

It is instructive to compare the SEEBL with other approaches in the literature. Thorpe and Nash (1984) solved a version of the SEE with an Ekman pumping bottom boundary condition for mid-latitude frontal scenarios. Their formulation did not permit a variable boundary layer depth or a full representation of the advection of momentum and buoyancy within the boundary layer as allowed in the SEEBL. Smith and Montgomery (2008) formulated the SEE in cylindrical polar coordinates for a hurricane boundary layer. However, the balance applied throughout was gradient-wind balance with no modification for the boundary layer drag. The boundary-layer friction was applied as a forcing on the right hand side of the SEE.

The Ekman pumping formula is a popular method of determining the impact of the boundary layer on the larger scale. Here, Ekman momentum balance is assumed, which in our 2D system appears as the following in the y direction:

$$fu = -\frac{\partial\overline{v'w'}}{\partial z} \tag{3.6}$$

where $\overline{v'w'}$ is the boundary-layer momentum flux in the y-direction. Integrating continuity (Eq. 2.5) over the depth of the boundary layer gives the vertical velocity at the top of the boundary layer (w_h). Also assuming that the boundary layer depth does not vary with x then gives the standard formula:

$$w_h = -\frac{1}{f}\frac{\partial\overline{v'w'}_0}{\partial x} \tag{3.7}$$

where the subscript 0 indicates the near-surface values. Compared with the SEEBL (Eq. 3.1), Equation (3.7) neglects the advection of momentum and buoyancy, and the variation of boundary layer depth in the horizontal. The SEEBL also explicitly includes the surface heat flux via the buoyancy equation (Eq. 2.4), unlike the Ekman pumping formula.

4. A baroclinic low-level jet case

In order to demonstrate the performance of the SEEBL, we require a large-scale meteorological case with substantial momentum and buoyancy advection as well as considerable forcing from boundary layer processes. A baroclinic low-level jet case provides all of these ingredients. Furthermore, the frontal scenario was the original motivation for the SEE (Sawyer, 1956; Eliassen, 1962), so it will also be interesting to see how the SEEBL performs in this setting. We first give an example of such a jet from analyses, and then design an idealised version inspired by this case. The idealised case consists of an isolated 2D low-level jet and allows a straightforward calculation of all the terms in the SEEBL. We finally show the circulations diagnosed with the SEEBL, along with the sensitivity to the momentum and buoyancy advection terms.

(*a*) *Analysed case*

Figure 2 shows ECMWF ERA-interim analyses (Dee *et al.*, 2011) of a mature mid-latitude cyclone in the West Atlantic on 0Z 22 December 2008, at latitude 52 N. Figure 2a shows a significant low-level jet in the centre of the cross-section with a maximum at 1 km height. The jet is associated with the cold converyor belt. The jet also leans to the left with height consistent with the frontal structure (Fig 2b). The jet maximum is within the boundary layer. The baroclinicity is indicated by the horizontal gradient of potential temperature (cold to the left, warm to the right). The baroclinic zone within the boundary layer is about 300 km wide. The potential temperature cross section shows a weakly stratified boundary layer to the left (cold side) of the cold front. The boundary layer is more stratified to the right of the front.

(*b*) *Idealised jet*

We aim to reproduce the key features of the analysed low-level wind jet and isolate its impact on the boundary layer circulation. Of course, our two-dimensional setting will not capture horizontal curvature effects of the analysed case. However, basing the idealised jet on the vertical cross-section will ensure the scales used are physically realistic. First we want the jet to lean with height, consistent with a frontal surface. We then want the geostrophic wind to peak near the surface, as this will drive the boundary layer state. Finally we want the horizontal shear to be greater on the right side of the jet, and the horizontal and vertical scales of the jet to be consistent with the analysis. These features are achieved by the following geostrophic wind in the y-direction:

$$v_g(\hat{x},\hat{z}) = V_0 exp\left[-\left(\frac{c}{c_j}\right)^2\right] exp\left(-\frac{\hat{z}}{d_j}\right)\left[1+tanh\left(-\frac{\hat{x}}{e_j}\right)\right]$$

$$\hat{x}=\frac{x}{L_d} \qquad \hat{z}=\frac{z}{H_d} \qquad c=\hat{x}+\alpha\hat{z} \tag{4.1}$$

where $V_0 = -30$ ms^{-1}, $c_j = 0.15$, $d_j = 0.225$, $e_j = 0.0625$, $\alpha = 0.3$. The domain width ($2L_d$) was 4000 km, and domain height (H_d) 20 km. A horizontal grid length of 31 km and constant vertical grid length of 156 m were used. The potential

(a)

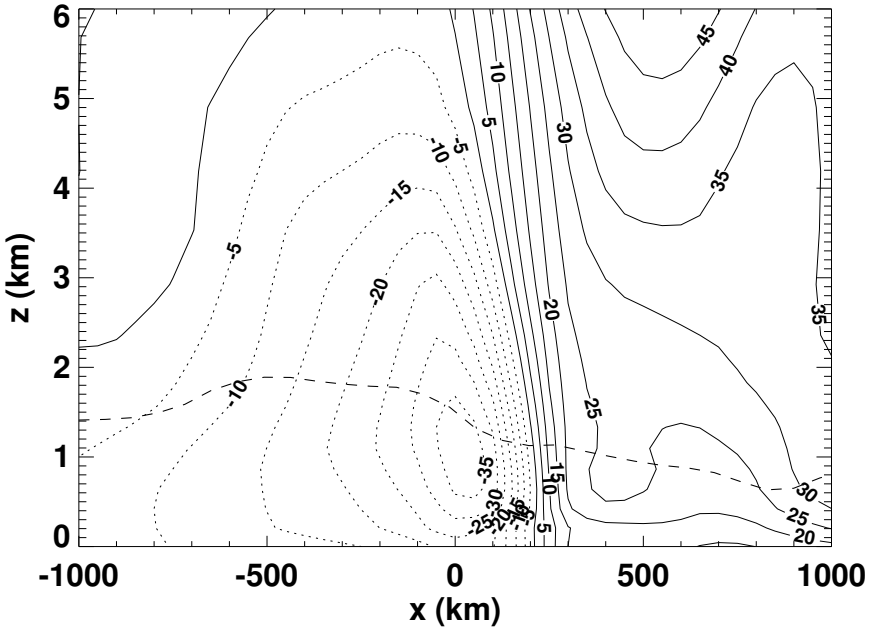

(b)

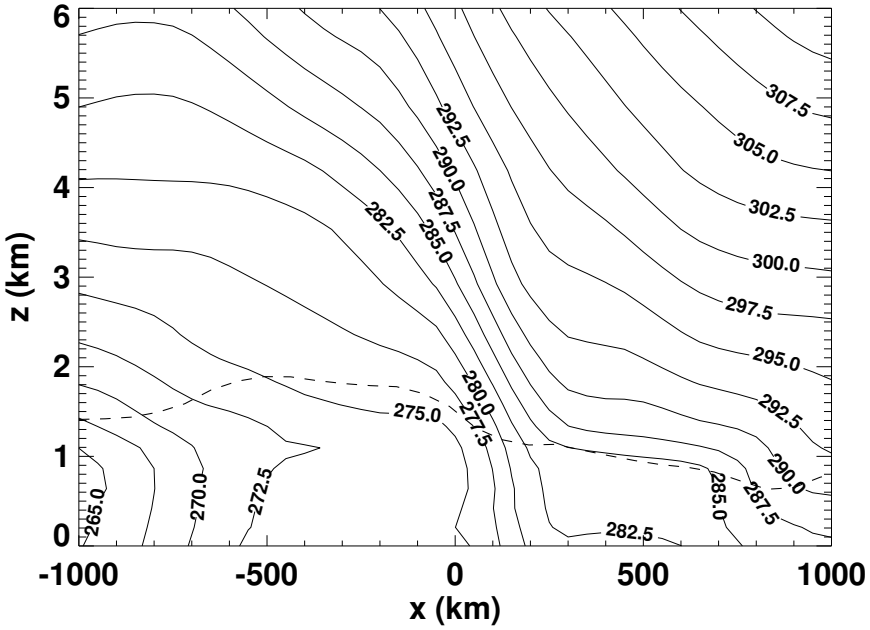

Figure 2. Vertical cross-sections of a mid-latitude cyclone low-level jet from ERA-interim analyses. Cross-sections shown at constant latitude starting at point (52N, 45W) for 0Z on 22/12/08: (a) wind in the North-South direction, contour interval 5 ms^{-1}, negative values dotted, (b) potential temperature (contour interval 2.5 K). Boundary-layer depth dashed.

temperature was initialised using thermal wind balance. The initial surface potential temperature was equal to the value at the first grid-level above the surface. The boundary-layer parametrization defined in section 2 was used, along with surface exchange scheme of Beljaars and Holtslag (1991). The boundary-layer scheme was integrated with the geostrophic and potential temperature initial conditions. The geostrophic wind and the surface temperature were kept at their initial values throughout the integration. By 6 hours, the boundary-layer diffusion settled to an equilibrium value. We determine the Ekman-balanced wind for a given K_m and $\frac{\partial \phi}{\partial x}$ using the matrix inversion method described by Beare and Cullen (2010).

Figure 3a shows the Ekman-balanced wind in the y direction (v_e) along with the boundary-layer depth. The boundary-layer depth is diagnosed as the height above which the gradient Richardson number is greater than one. The jet peaks at height 1 km, below the boundary layer top, similar to that in Fig. 2a. The boundary layer depth increases to a maximum of 1600 m, corresponding to the region of maximum wind speed. This is due to the boundary-layer turbulence being driven by the wind shear. Since we are considering an isolated jet, the variation of boundary layer depth is more significant than in Fig. 2. Above the boundary layer, v_e is, by definition, the same as the geostrophic wind. The baroclinic structure (Fig. 3b) above the boundary layer is similar to Fig. 2b. The boundary layer is strongly stratifed to the right, but weakly stratified to the left of the domain. Again, this is similar to Fig. 2b, although it is more well-mixed to the left. The horizontal scale of the strongest baroclinic zone (about 300-400 km) is similar to Fig. 2b. The frontal surface in Fig. 3b is less inclined than in Fig. 2b. In summary, although the idealised case does not reproduce the analysed case exactly, many of the key physical features are consistent between the two.

Figure 4a shows the Ekman-balanced wind in the x-direction (u_e). It is slightly negative near the boundary-layer top and increases to a maximum value of 17 ms^{-1} in the same horizontal location but below where the low-level jet peaks in Figure 3a. The profiles of u_e and v_e (Fig. 3a) correspond to the familiar turning of the wind within the boundary layer, with the wind backing when moving down through the boundary layer. The boundary layer diffusion (K_m, Fig. 4b) follows u_e closely with a maximum below the middle of the boundary layer.

(*c*) *SEEBL circulations*

Figure 5a shows the stream function diagnosed using the SEEBL (Eq. 3.1). The potential temperature is shown alongside for reference (Fig. 5b). The stream function shows an anti-clockwise circulation which is strongest just below the boundary-layer top. There is also a tilt to the left in the axis of the circulation. This is consistent with the effect of baroclinicity seen in SEE calculations (Hakim and Keyser, 2001).

The velocity components diagnosed by the SEEBL are shown in Figure 6. Figure 6a shows a positive advecting velocity (u) within the boundary layer with a negative return flow near the boundary-layer top. The magnitude of the advecting velocity is larger than the Ekman-balanced velocity (Fig. 4) near the bottom and the top of the boundary layer. The advecting velocity is also phase-shifted by 200 km to the left relative to the Ekman-balanced velocity. The pattern is due

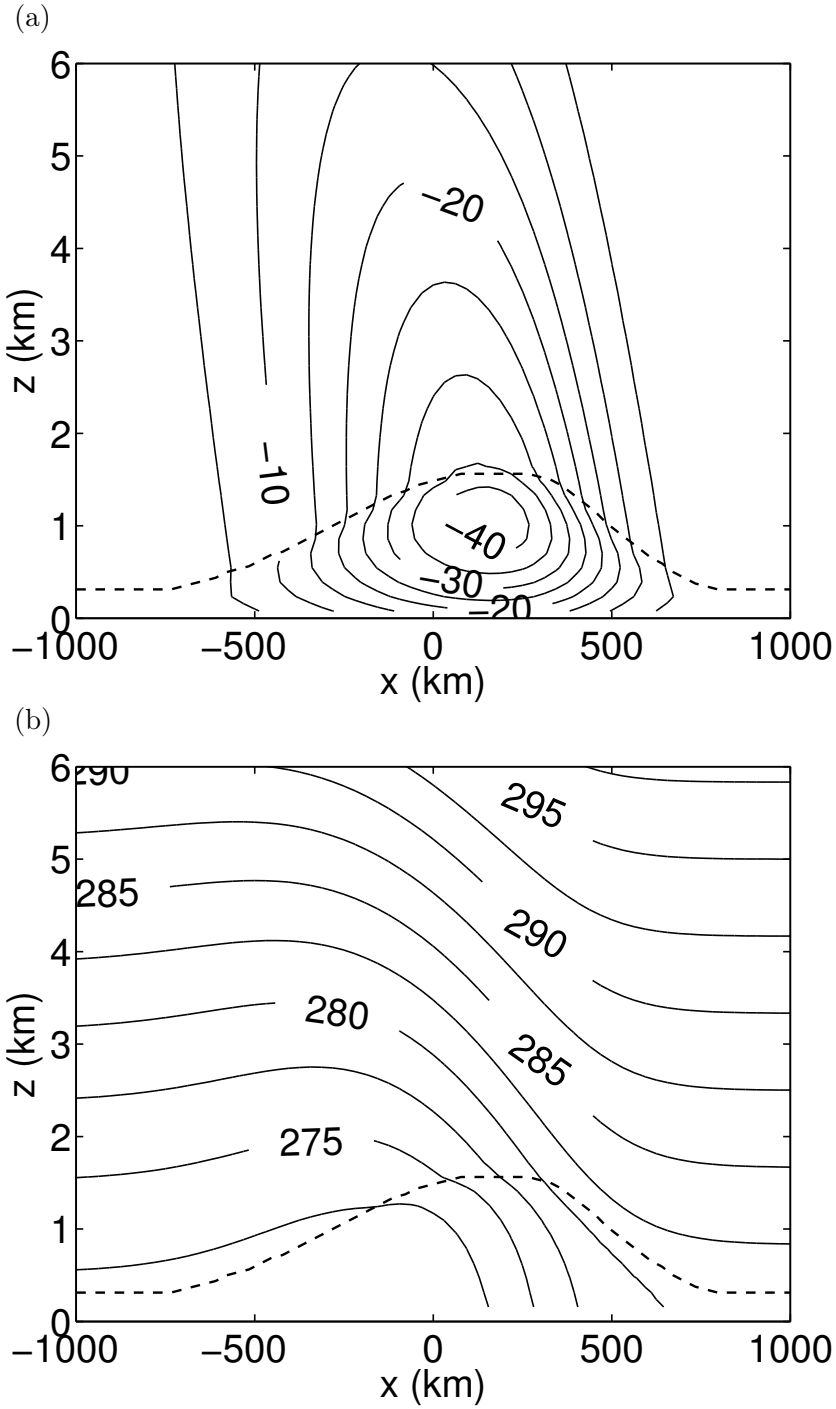

Figure 3. Vertical cross-sections of: (a) The Ekman-balanced wind in the north-south direction (contour interval 5 ms^{-1}), (b) the potential temperature (contour interval 2.5 K) resulting from the thermal wind balance initialisation followed by 6 hours of integration of the boundary-layer scheme. Boundary-layer depth dashed.

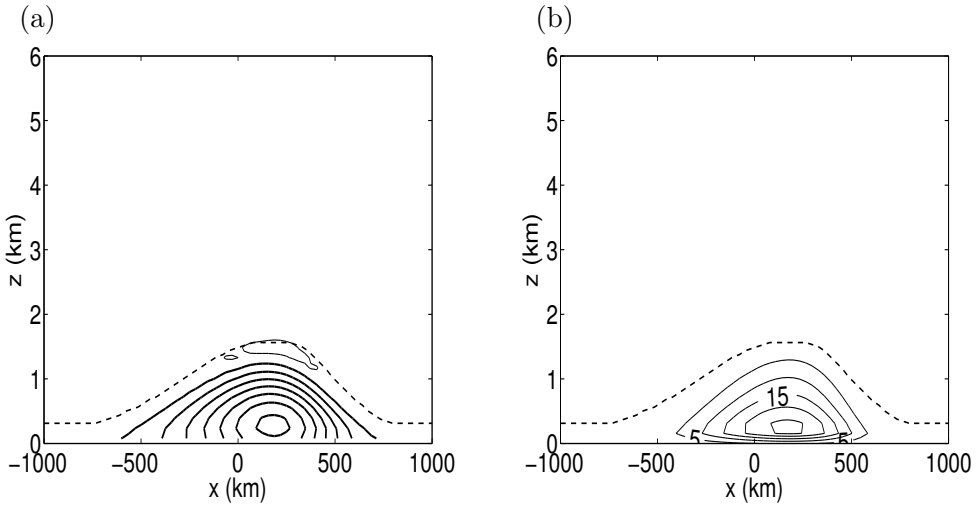

Figure 4. (a) Ekman-balanced wind in the x-direction, u_e (contour interval 2.5 ms^{-1}, bold positive, feint negative, zero contour omitted for clarity) and (b) boundary-layer momentum diffusivity (contour interval 5 $\mathrm{m}^2\mathrm{s}^{-1}$). Boundary-layer depth dashed.

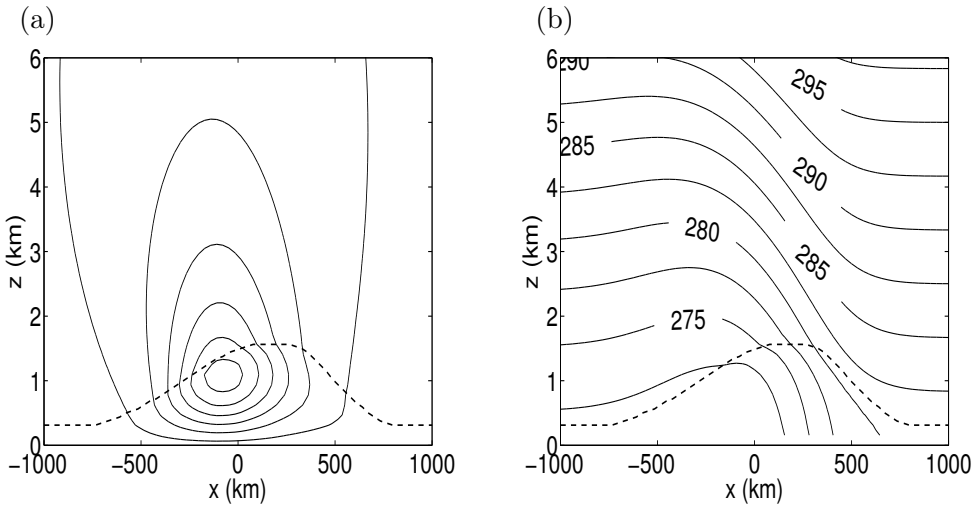

Figure 5. (a) Stream function (contour interval 3000 $\mathrm{m}^2\mathrm{s}^{-1}$, outermost contour is 1500) diagnosed by the SEEBL and (b) potential temperature (contour interval 2.5 K). Boundary-layer depth dashed.

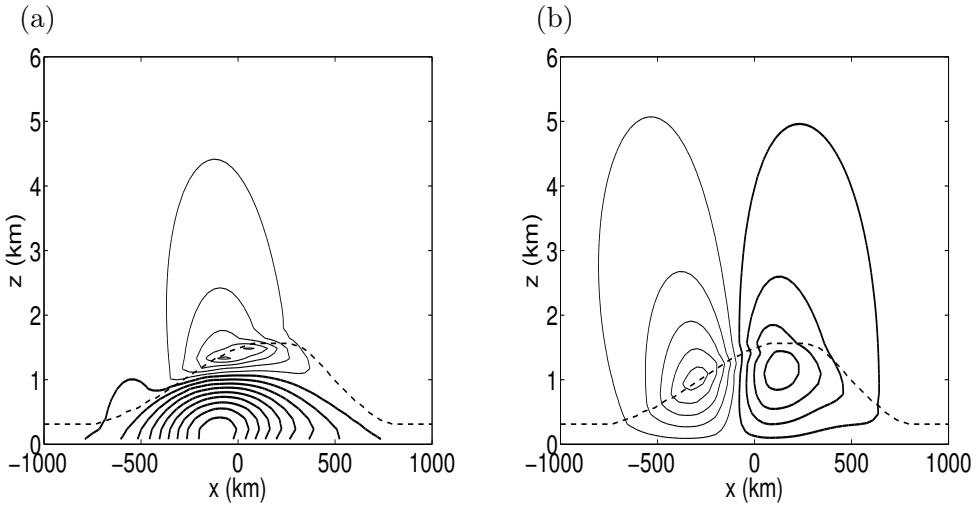

Figure 6. (a) Advecting velocity u (contour interval 2.5 ms^{-1}) and (b) vertical velocity (contour interval 1 cms^{-1}) diagnosed by SEEBL. Positive values bold, negative values feint, zero contour omited for clarity. Boundary-layer depth dashed.

to the momentum and buoyancy advection terms along with the enforcement of continuity in the SEEBL.

The vertical velocity pattern (Fig. 6b) accounts for the variation of the boundary-layer depth. There are sloping regions of descent and ascent to the left and right respectively of the jet maximum. The region of descent follows the boundary-layer top closely whilst the region of ascent is slightly below and to the left of the downward sloping boundary layer top. The magnitude of the maximum ascent is smaller than the magnitude of the maximum descent: the maximum vertical velocity is 4.1 cms^{-1} and minimum value is -5.5 cms^{-1}. In contrast, the Ekman pumping formula (Eq. 3.7) diagnoses a maximum vertical velocity of 3.8 cms^{-1} and minimum value of -2.6 cms^{-1}. The Ekman pumping thus has the reverse pattern of maximum ascent and maximum descent from the SEEBL and follows the horizontal vorticity of the jet. However, the SEEBL includes the additional significant effects of a sloping boundary layer and momentum and buoyancy advection.

Figure 7 compares the advecting velocity v (diagnosed from Eq. 3.5) with the Ekman-balanced wind v_e. The v wind has a jet that is significantly larger in magnitude than v_e (by up to 6.5 ms^{-1}). This is a reflection of the momentum advection terms being a significant component of the dynamics (see Eq. 3.5). Combined with Fig. 6a, this shows that the full advecting velocity (u, v) has a larger magnitude than the Ekman-balanced velocity (u_e, v_e).

The SEEBL diagnosis was explored further by performing two tests of sensitivity to its coefficients. Figure 8a shows the vertical velocity diagnosed by the SEEBL when the advection of the Ekman-balanced velocity and horizontal buoyancy advection terms are removed (this corresponds to removing the terms in $\frac{\partial u_e}{\partial x}$, $\frac{\partial v_e}{\partial x}$, $\frac{\partial^2 \psi}{\partial x \partial z}$, $\frac{\partial \psi}{\partial x}$ and $\frac{\partial \psi}{\partial z}$ in Eq. 3.1). The vertical velocity pattern is approximately 50% weaker, and the asymmetry between ascent and descent is now

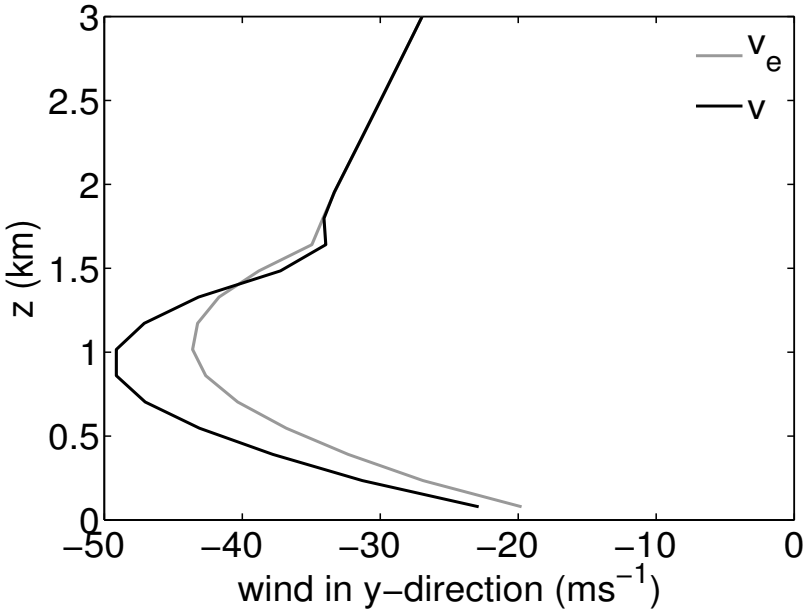

Figure 7. Vertical profiles of v_e (grey) and v (black) at the horizontal location of the jet maximum.

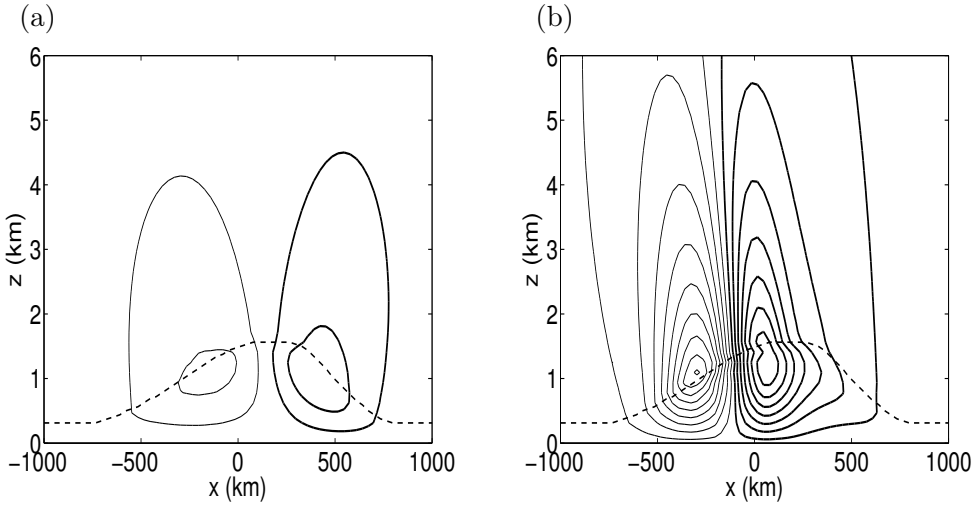

Figure 8. Vertical velocity (contour interval 1 cms^{-1}) when: (a) momentum advection and horizontal buoyancy advection terms are neglected in the SEEBL, (b) stratification is set to quarter its value in SEEBL. Positive values bold, negative values feint and zero contours omited for clarity. Boundary-layer depth dashed.

small and slightly reversed. Figure 8b shows the effect of reducing the stratification (N^2) by a factor of four. This amplifies the circulation by a factor of two, and increases the vertical extent of the circulation (consistent with a scale height for the stream function which varies as $1/N$).

5. Discussion

Since the seminal papers of Sawyer (1956) and Eliassen (1962), an important aspect of dynamical meteorology has been determining the vertical circulations, particulary in frontal zones. The Sawyer-Eliassen equation (SEE) arises out of the semi-geostrophic theory of Hoskins (1975). Several authors (e.g. Thorpe and Nash, 1984; Smith and Montgomery, 2008) have incorporated the effects of the boundary layer in the SEE by either the bottom boundary condition or external forcing. However, there has yet to be an explicit treatment of the momentum and thermodynamic balances within the boundary layer, or an accounting of the variation of the boundary-layer depth in space.

In this paper we described a new methodology for diagnosing circulations forced by the boundary layer coupled to the large-scale dynamics. We derived the analogue of the semi-geostrophic equations for the boundary layer. These were called the semi-geotriptic (SGT) equations and used Ekman balance in the place of geostrophic balance. We then formulated a Sawyer-Eliassen type of elliptic equation for the stream function in the vertical plane from the SGT equations, which now explicitly included boundary-layer vertical diffusion (SEEBL).

We showed example numerical solutions of the SEEBL for a baroclinic low-level jet. The circulation from the SEEBL closely followed the significant variation of the boundary-layer depth acoss the front. The circulation had more descent on the anticyclonic side of the jet than ascent on the cyclonic side; such symmetry was opposite from that predicted by the Ekman pumping. The symmety of the SEEBL's circulation is also in agreement with Bannon (1998) who considered just the boundary-layer momentum budget, and showed that the Ekman pumping overestimates the maximum ascent in cyclonic regions but underestimates the maximum descent in anti-cyclonic regions. Whilst the Ekman pumping assumes a steady-state momentum balance, the SEEBL also includes advection of momentum and buoyancy and permits variable boundary layer depth. We showed that the net effect of including advection of momentum and horizontal advection of buoyancy was a significant enhancement of the vertical circulation. We also identified vertical advection of buoyancy as a significant control on the depth and strength of the circulation.

The SGT equations have revealed a distinct mechanism for low-level jets from the commonly used inertial oscillation. The jet is enhanced from the Ekman-balanced state due to the contribution from momentum advection. However, unlike the inertial oscillation jet (e.g. Ostdiek and Blumen, 1997), the jet is 'slaved' to the balanced wind and doesn't behave in an unbalanced or oscillatory way (Fig. 7). The SGT equations also provide an explanation of why the low-level jet is found to be significantly ageostrophic (Akiyama, 1973). The SGT equations thus provide some new elements of a comprehensive dynamical description of low-level jets.

The benefits of our methodology are not limited to the atmosphere. Samelson and Vallis (1997) showed that the frictional planetary geostrophic model has benefit in the oceans. In the same vein, the SEEBL could be adapted to incorporate the interaction of the ocean mixed layer with the ambient dynamics. It could thus prove to be a valuable tool for diagnosing the interaction of the boundary layer with the large-scale dynamics throughout the climate system.

References

Akiyama, T. (1973). Ageostrophic low level jet stream in the Baiu season associated with heavy rainfalls over the sea area. *J. Meteor. Soc. Japan*, **51**, 205–208.

Back, L. E. and Bretherton, C. S. (2009). On the relationship between SST gradients, boundary layer winds, and convergence over the tropical oceans. *J. Climate*, **22**, 4182–4196.

Bannon, P. R. (1998). A comparison of Ekman pumping in approximate models of the accelerating Planetary Boundary Layer. *J. Atmos. Sci.*, **55**, 1446–1451.

Beare, R. J. (2007). Boundary layer mechanisms in extratropical cyclones. *Quart. J. Roy. Meteorol. Soc.*, **133**, 503–515.

Beare, R. J. and Cullen, M. J. P. (2010). A semi-geostrophic model incorporating well-mixed boundary layers. *Quart. J. Roy. Meteorol. Soc.*, **136**, 906–917.

Beare, R. J. and Cullen, M. J. P. (2012). Balanced models of boundary-layer convergence. *to appear Quart. J. Roy. Meteorol. Soc.*

Beljaars, A. C. M. and Holtslag, A. A. M. (1991). Flux parameterization over land surfaces for atmospheric models. *Journal of Applied Meteorology*, **30**, 327–341.

Chen, G. T.-J., Wang, C.-C., and Lin, D. T.-W. (2005). Characteristics of low-level jets over Northern Taiwan in Mei-Yu season and their relationship to heavy rain events. *Mon. Wea. Rev.*, **133**, 20–43.

Clark, P. A., Browning, K. A., and Wang, C. (2005). The sting at the end of the tail: Model diagnostics of fine-scale three-dimensional structure of the cloud head. *Quart. J. Roy. Meteorol. Soc.*, **131**, 2263–2292.

Dee, D. P., Uppala, S. M., Simmons, A. J., Berrisford, P., Poli, P., Kobayashi, S., Andrae, U., Balmaseda, M. A., Balsamo, G., Bauer, P., Bechtold, P., Beljaars, A. C. M., van de Berg, L., Bidlot, J., Bormann, N., Delsol, C., Dragani, R., Fuentes, M., Geer, A. J., Haimberger, L., Healy, S. B., Hersbach, H., Holm, E. V., Isaksen, L., Kallberg, P., Kohler, M., Matricardi, M., McNally, A. P., Monge-Sanz, B. M., Morcrette, J.-J., Park, B.-K., Peubey, C., de Rosnay, P., Tavolato, C., Thepaut, J.-N., and Vitart, F. (2011). The ERA-Interim reanalysis: configuration and performance of the data assimilation system. *Quart. J. Roy. Meteorol. Soc.*, **137**, 553–597.

Eliassen, A. (1962). On the vertical circulation in frontal zones. *Geophys. Publ.*, **24**, 147–160.

Hakim, G. J. and Keyser, D. (2001). Canonical frontal circulation patterns in terms of Green's functions for the Sawyer-Eliassen equation. *Quart. J. Roy. Meteorol. Soc.*, **127**, 1795–1814.

Hoskins, B. J. (1975). The Geostrophic Momentum approximation and Semi-Geostrophic equations. *J. Atmos. Sci.*, **33**, 233–242.

Louis, J. F. (1979). A parametric model of vertical eddy fluxes in the atmosphere. *Boundary-Layer Meteorol.*, **17**, 187–202.

Ostdiek, V. and Blumen, W. (1997). A dynamic trio: Inertial oscillation, deformation frontogenesis. *J. Atmos. Sci.*, **54**, 1490–1502.

Pedlosky, J. (1987). Geophysical Fluid Dynamics. *Springer; 2nd ed. 728pp.*

Samelson, R. M. and Vallis, G. K. (1997). A simple friction and diffusion scheme for Planetary Geostrophic basin models. *Journal of Physical Oceanography*, **27**, 186–194.

Sawyer, J. S. (1956). The vertical circulation at meteorological fronts and its relation to frontogenesis. *Proc. R. Soc. London.*, **A234**, 346–362.

Smith, R. K. and Montgomery, M. T. (2008). Balanced boundary layers used in hurricane models. *Quart. J. Roy. Meteorol. Soc.*, **134**, 1385–1395.

Thorpe, A. J. and Nash, C. A. (1984). Convective and boundary layer parametrizations in a diagnostic model of atmospheric fronts. *Quart. J. Roy. Meteorol. Soc.*, **110**, 443–466.